Direct Measurement of the Damping of Toroidicity-Induced Alfvén Eigenmodes

A. Fasoli,[1,2] D. Borba,[1] G. Bosia,[1] D. J. Campbell,[1] J. A. Dobbing,[1] C. Gormezano,[1] J. Jacquinot,[1] P. Lavanchy,[1,2] J. B. Lister,[1,2] P. Marmillod,[1,2] J.-M. Moret,[1,2] A. Santagiustina,[1] and S. Sharapov[1]

[1]*JET Joint Undertaking, Abingdon, Oxon OX14 3EA, United Kingdom*

[2]*Centre de Recherches en Physique des Plasmas, Association EURATOM-Confédération Suisse, Ecole Polytechnique Fédérale de Lausanne, 1015 Lausanne, Switzerland*

(Received 30 January 1995)

This Letter presents the first direct experimental measurements of the damping of toroidicity-induced Alfvén eigenmodes (TAE), carried out in the JET tokamak. These measurements were obtained during the first experiments to drive these modes with antennas external to a tokamak plasma. Different regimes corresponding to different dominant TAE absorption mechanisms with a wide range of damping rates, $10^{-3} \leq \gamma/\omega \leq 10^{-1}$, have been identified in Ohmically heated plasma discharges.

PACS numbers: 52.35.Bj, 52.55.Fa, 52.55.Pi

In ignited magnetically confined plasmas, the large amount of energy and the steep pressure gradients associated with alpha particles created by fusion reactions can lead to the excitation, via wave-particle interactions, of global electromagnetic modes, which may be deleterious for plasma performance. Of particular concern in tokamaks are Alfvén eigenmodes, which exist in the gaps of the shear Alfvén wave continua, induced by toroidal geometry (TAE) [1], elliptical cross section (EAE) [2], and finite pressure effects (BAE) [3,4]. These modes can be driven by resonant fast particles, with velocities $v \sim v_{\text{Alfvén}}$ [$v_{\text{Alfvén}} = B_{\text{tor}}/(\mu_0\rho)^{1/2}$, ρ being the mass density, and B_{tor} the toroidal magnetic field], and may affect the orbits of the resonant particles themselves, creating anomalous transport [5]. The resonance condition may apply to ions accelerated by neutral beam injection (NBI) or ion cyclotron resonance heating (ICRH), but, more importantly, is inevitably satisfied by fusion created alpha particles during their slowing down. By enhancing alpha-particle transport, Alfvén eigenmodes may thus lead to an increase of the reactivity required for ignition, as well as to localized energy deposition and significant first wall damage [6].

In order to assess the linear stability of Alfvén eigenmodes, both driving and damping effects must be investigated. The theoretical evaluation of these terms is made extremely intricate by the concurrence of MHD and kinetic effects. Predicted damping rates vary by more than 1 order of magnitude, according to the *a priori* assumptions characterizing different models. Existing experimental results on the role of the Alfvén eigenmodes in affecting transport also vary considerably. TAE, BAE, and, possibly, EAE activity driven by energetic particles has been reported for NBI and ICRH heated discharges in different tokamak experiments [4,7–10]. Fast particle losses together with a sudden reduction of the neutron production rate have been observed at the same time as bursts of TAE activity [6]. In similar experiments in deuterium-tritium plasmas, no increase in the lost alpha flux was observed in the presence of TAE activity [11]. Such passive studies, although providing frequency and mode spectra as well as some information on the instability thresholds, cannot provide quantitative estimates of the damping and driving of the Alfvén eigenmodes.

A more complete picture of the MHD activity in this Alfvén range of frequencies, and, specifically, insight into the Alfvén eigenmode absorption mechanisms based on direct measurements of the mode damping rate, can be obtained from an analysis of the plasma response to external perturbations. Combining excitation by external antennas with coherent detection of various probing signals at the plasma edge and in the core has created the active diagnostic for Alfvén eigenmodes on the JET tokamak [12]. Similar experiments had previously only been carried out in the discrete Alfvén wave range of frequencies on the TCA, PETULA, and TEXTOR tokamaks [13–15]. In this Letter we present the experimental arrangement and method, results on the identification of the eigenmode dispersion relation, and the first measurements of the damping rate for toroidicity-induced Alfvén eigenmodes.

The JET saddle coils, four above and four below the plasma, situated inside the vacuum vessel 90° apart toroidally, are used as external antennas to excite the Alfvén eigenmodes. The exciter and detection systems cover the frequency range from 20 to 500 kHz, including BAE, TAE, and EAE. The exciter comprises a remotely controllable function generator, a 3 kW broadband power amplifier, a broadband matching network, a power splitter, and an isolation unit. The power distribution unit can drive one, two, or four saddle coils with different phase combinations to preferentially excite specific, low toroidal mode numbers (n) and poloidal symmetry. Maximum current and voltage applied to the saddle coils are of the order of 30 A and 500 V. The corresponding magnetic perturbations in the plasma are calculated to be small, $\delta B/B_{\text{tor}} < 10^{-5}$ [16,17], and are expected neither to generate significant transport of energetic particles nor to produce any nonlinear wave effects.

The diagnostic method requires repetitive sweeps of the driving frequency in the region of the Alfvén continuum gap frequency. The driven plasma response is extracted from background noise in various diagnostic signals using synchronous detectors which provide the in phase and quadrature, i.e., the real and imaginary, components of the signals. The voltage induced on the unexcited saddle coils and the pickup coils measure the perturbed radial and poloidal magnetic fields at several locations, allowing a mode analysis in the poloidal and toroidal conjugate plane.

Several global eigenmodes have been clearly observed in different plasma conditions, during the Ohmic phase of JET deuterium discharges in the range 60–180 kHz. An example of a resonance detected on one of the magnetic field probes is shown in Fig. 1. The signal describes a circle in the complex plane as the frequency is swept across the resonance. The maximum value of the oscillating magnetic field measured by the coil is of the order of 10^{-7} T for driving currents of the order of 5 A in each antenna.

The transfer function between the driving current and any particular diagnostic signal can be directly derived from the raw data by dividing that signal by the antenna current. The presence of an Alfvén eigenmode manifests itself as a resonance in this transfer function H, which can be represented in terms of complex conjugate poles, p_k and p_k^*, and residues, r_k and r_k^*,

$$H(\omega,x) = \sum_{k=1}^{N} \frac{1}{2}\left(\frac{r_k(x)}{i\omega - p_k} + \frac{r_k^*(x)}{i\omega - p_k^*}\right) + D(\omega,x) = \frac{B(\omega,x)}{A(i\omega)}.$$

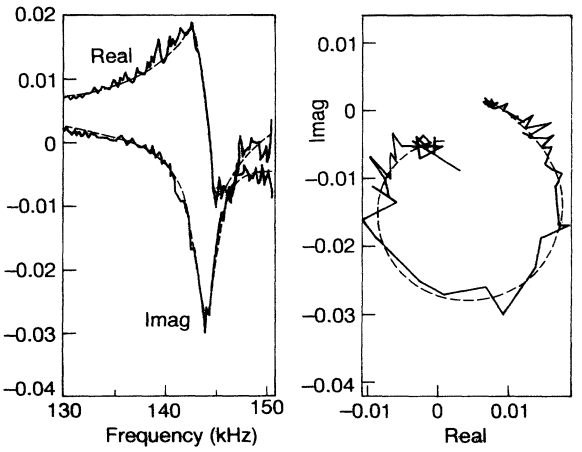

FIG. 1. Example of a TAE resonance in the Ohmic phase of JET shot No. 31638. Real and imaginary parts (left) and complex plane representation (right) of a magnetic probe signal, normalized to the driving current. The fit with B and A of order 5 and 2 is also shown, giving $f_{\text{obs}} = 144.2 \pm 0.1$ kHz, $\gamma/2\pi = 1400 \pm 100$ s^{-1}. $B_{\text{tor}} \cong 2.8$ T, $I_p \cong 2.2$ MA, and $\bar{n}_e \cong 3 \times 10^{19}$ m^{-3}; the two upper saddle coils were used in phase and 180° apart toroidally.

Here N is the number of resonances in the measurement range, ω the driving frequency, and x the measurement position. For the kth resonance, $p_k = i\omega_{0k} + \gamma_k$ defines a pole which is common to all diagnostic signals, with ω_{0k} being the resonance (real) frequency and γ_k the damping rate. Since the signals may contain a direct, nonresonant coupling with the antenna, an additional scalar quantity D is added to the first order resonance terms.

The data from a complete set of diagnostic signals are analyzed by simultaneously fitting the above expression to all of the signals, with a single denominator A, which determines the resonance characteristics, and separate numerators B [18]. The imaginary part of the fitted pole gives the frequency of the mode, $f_{\text{obs}} = \omega_{0k}/2\pi$. Its real part, in the case of stable modes, is the difference between the damping rate and the growth rate: $\gamma = \gamma_{\text{damping}} - \gamma_{\text{drive}}$. In particular, if no fast particle driving terms are present in the plasma, $\gamma_{\text{drive}} = 0$ and γ correspond directly to the damping rate of the mode, which is the case of the data shown in Fig. 1. For those signals that are space-resolved measurements of the wave field, the residues correspond directly to the wave amplitude as a function of space, i.e., to the single mode structure.

The result of this fitting procedure is shown in Fig. 1 superimposed on the raw signals. With numerator and denominator chosen of order 5 and 2, the fit provides an accurate value for the eigenmode frequency, $f_{\text{obs}} = 144.2 \pm 0.1$ kHz, and for its damping rate $\gamma/2\pi = 1400 \pm 100$ s^{-1}, corresponding to a relatively large resonance quality factor $Q = \omega/\gamma \sim 125$ or, equivalently, to a relatively weak damping $\gamma/\omega \sim 0.8\%$.

The "Alfvén" character of the measured resonances was verified from the dependence of their frequency on the magnetic field, plasma density, and current. Figure 2 shows an example of a discharge in which the toroidal magnetic field was varied from 2.2 to 3.0 T. The measured frequency agrees well with the value corresponding to the center of the toroidicity-induced gap, $f_{\text{TAE}}^0 \cong v_{\text{Alfvén}}/4\pi qR_0$, where q is the safety factor and R_0 is the tokamak major radius. Here f_{TAE}^0 is evaluated assuming $q = 1.5$, corresponding to the most effectively driven TAE mode [16,17], and using the line-averaged plasma density ($\bar{n}_e$) for calculating $v_{\text{Alfvén}}$. The value of γ/ω remained roughly constant at $\gamma/\omega \sim 1\%$. In other discharges the plasma density was varied. The mode frequency always followed f_{TAE}^0, with an inverse dependence on the square root of the density. These observations clearly demonstrate that the driven resonances are toroidicity-induced Alfvén eigenmodes.

The reconstruction of the TAE mode structure in the poloidal and toroidal directions is shown in Fig. 3, for a discharge with two upper saddle coils driven in phase, situated 180° apart toroidally, providing mostly $|n| = 2$ excitation. The phase of the residue of the response of the magnetic probes has a clear $|n| = 2$ standing wave structure. The $n = +2$ and $n = -2$ components are

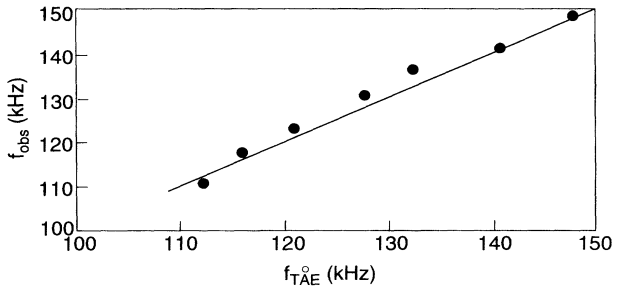

FIG. 2. Variation of the measured eigenmode frequency with toroidal magnetic field in JET shot No. 31591. B_{tor} varied linearly with time between 2.2 and 3 T; density and plasma current were kept constant; and the same saddle coils as in Fig. 1, but with opposite phase.

excited with identical amplitudes, the toroidal symmetry being maintained both by the excitation and by the plasma itself in the absence of significant toroidal rotation. The poloidal mode structure indicates a nodal point at the tokamak midplane, in agreement with theoretical estimates for typical TAE spatial field structures [16,17].

Several possible damping mechanisms for TAE modes have been proposed. First, continuum damping occurs when the eigenmode frequency intersects a shear Alfvén wave continuum at a resonant layer within the plasma. The damping is independent of the details of the absorption mechanisms for the continuum itself but is very sensitive to the profiles $q(r)$ and $\rho(r)$, where r is the minor radius of the magnetic surfaces on the tokamak midplane. Specifically, as the gaps are centered at the local value of f^0_{TAE}, continuum damping is linked to the radial dependence of the quantity $g = 1/q\rho^{1/2}$. If $g(r)$ is approximately constant, the gaps are aligned and the continuum damping should be minimized. If g varies strongly with r, continuum damping should become dominant and lead to large damping rates, $\gamma/\omega \sim (5-10)\%$ [19,20]. Second, in the absence of strong continuum damping, several kinetic effects may become important. Landau damping effects are mainly due to the mode interaction with bulk ions and electrons, when $v_{th\|} \sim v_{Alfvén}$ or $v_{th\|} \sim v_{Alfvén}/3$. Ion Landau damping scales as $\gamma_i/\omega \propto \beta_i^{-3/2}\exp(-1/9\beta_i)$ [21], $\beta_j = n_j T_j/(B^2_{tor}/2\mu_0)$ being the ratio between the pressure of the species j ($j = 1, e$) and the magnetic field pressure. γ_i is negligibly small for the Ohmic discharges considered, whereas for these relatively cold and dense plasmas, $v_{th\|} \sim v_{Alfvén}$ and thus electron Landau effects can contribute significantly to the damping $\gamma_e/\omega \propto \beta_e v_{Alfvén}/v_{th\|}$ [5]. Damping can also be produced by trapped electron collisional absorption, yielding $\gamma^t_e/\omega \propto (\nu_e/\omega)^{1/2}[\beta_e q^2 + 0.1(\rho_s/\Delta_{TAE})^2]$ [22,23]. Here $\nu_e \sim n_e/T_e^{3/2}$ is the electron collision frequency $\rho_s^2 = 2T_e/m_i\omega_{ci}^2$ and $\Delta^2_{TAE} = (\pi^2/64)(r\varepsilon/m)^2$, with ω_{ci} being the ion cyclotron angular frequency, ε the tokamak inverse aspect ratio, and m the poloidal mode number. Finally, a contribution to the TAE absorption can come from radiative damping [24], which leads to

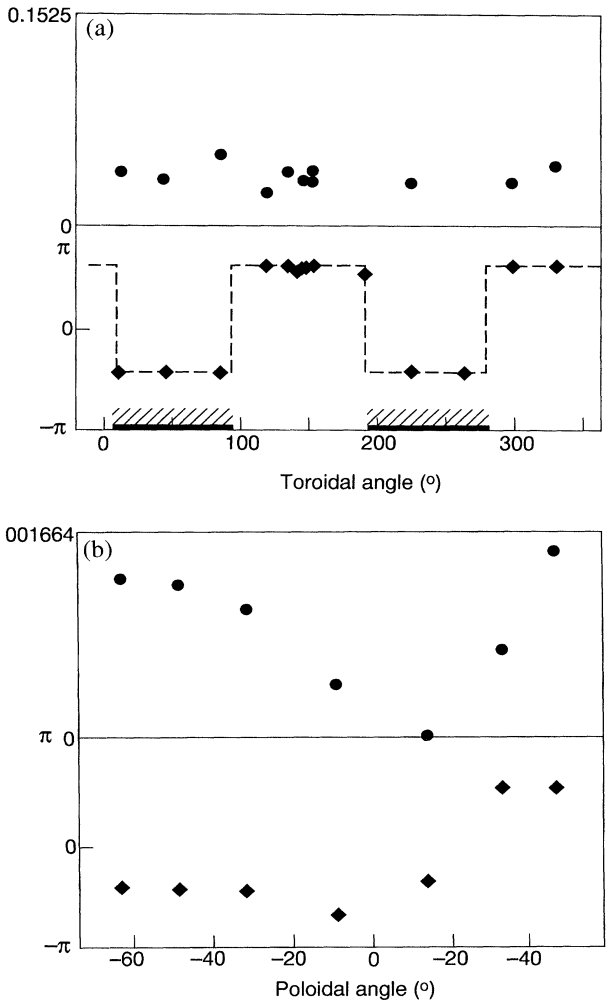

FIG. 3. Toroidal and poloidal mode structure of a TAE, represented as the magnitude (+) and phase (×) of the residues fitted to the poloidal field pickup coil signals, normalized to the active saddle coil current. The driven spectrum $|n| = 2$ and the plasma parameters were as in Fig. 1. The poloidal angle is measured from the tokamak outer midplane upward. The toroidal extension of the JET saddle coils is indicated as a shaded region. The poloidal angle for the toroidal array (top) is $\sim 47°$, while the toroidal angle for the poloidal array (bottom) is $\sim 17°$.

$\gamma_R/\omega \propto s^2\exp[-f(s,\varepsilon)/\rho_i m]$, where f is a function of the magnetic shear s [$s = (r/q)\,dq/dr$] and ε, and ρ_i is the ion Larmor radius.

Greatly differing damping rates were measured in two similar discharges with different $g(r)$. Figure 4 shows the radial dependence of $g(r)$ obtained from the reconstructed equilibrium and the density profiles, together with the two measured eigenmodes and their damping rates. When there was a strong radial dependence of $g(r)$, Fig. 4, curve (a), the gaps were not aligned through the continuum structure and strong damping occurred with $\gamma/\omega \sim 5\%$, in agreement with prior theoretical estimates of continuum damping [20]. The $g(r)$ profile in Fig. 4, curve (b),

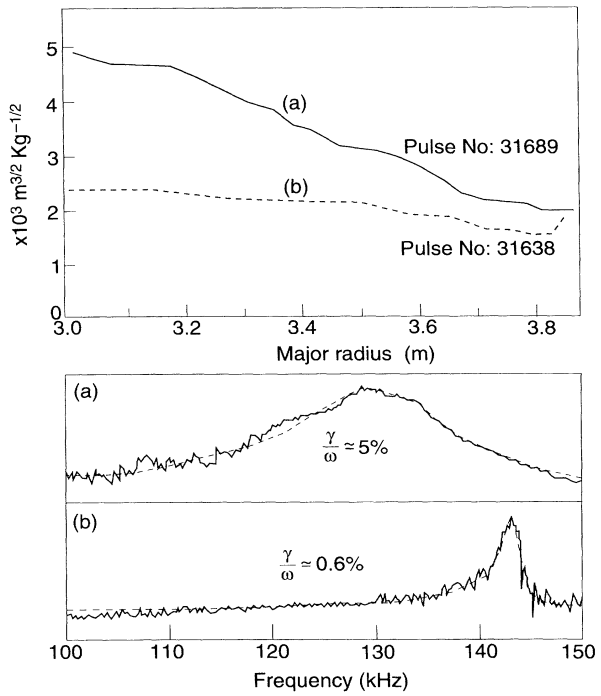

FIG. 4. The relationship between the profile of $g(r) = 1/q(r)\rho(r)^{1/2}$ and the TAE damping. $g(r)$ and the raw and fitted frequency responses of a normalized magnetic probe signal are shown for two discharges. Excitation peaked at $|n| = 2$ was used for both discharges; measurements were taken in the Ohmic phase with similar plasma configuration; $\overline{n}_e \cong 4 \times 10^{19}$ m^{-3}. (a) $B_{\text{tor}} \cong 1.8$ T, $I_p \cong 2$ MA. (b) $B_{\text{tor}} \cong 2.8$ T, $I_p \cong 2.3$ MA.

was flatter and led to a more "open" gap structure and therefore to a much less effective continuum damping. The absorption mechanism in this case has to be sought in the kinetic interactions.

Damping rates were measured in a wide variety of conditions, with $1 < I_p < 3$ MA, $1 \times 10^{19} < \overline{n}_e < 5 \times 10^{19}$ m^{-3}, and $1 < B_{\text{tor}} < 3.5$ T. The results with both odd and even low-n excitation span several orders of magnitude, from $\gamma/\omega < 0.1\%$ to $\gamma/\omega > 10\%$, suggesting that different absorption mechanisms dominate according to the configuration of each specific shot. This extreme sensitivity of the damping rates of the TAE to the details of the plasma equilibrium profiles makes comparisons with theoretical predictions very difficult. Even in the case of flat $g(r)$ profiles, the measured damping appears to be at least a factor of 2 larger than that calculated by local models considering electron Landau and electron collisional damping in the particular case of low mode numbers. Contributions from either continuum damping at the plasma edge or by radiative damping in the core must therefore be significant.

The successful implementation of a new active diagnostic for Alfvén eigenmodes, combining external excitation using the JET saddle coils as antennas with synchronous detection of the diagnostic response, has allowed us to drive and identify toroidicity-induced Alfvén eigenmodes in linearly stable conditions. Control of the antenna phasing together with space-resolved magnetic wave field measurements has permitted both the selection and the identification of the driven mode structure. The damping rates of the toroidicity-induced Alfvén eigenmodes have been experimentally measured for the first time. The large range of the measured values of γ/ω indicates the capability of the diagnostic method, highlights the effectiveness of different MHD and kinetic absorption mechanisms, and provides a useful test for the theories being developed to assess the stability of Alfvén eigenmodes in future ignition experiments.

The authors thank the members of the JET Team for experimental support. This work was partly supported by the Fonds National Suisse pour la Recherche Scientifique, within the JET/CRPP-EPFL Task Agreement 394.

[1] C.Z. Cheng, L. Chen, and M.S. Chanse, Ann. Phys. (N.Y.) **161**, 21 (1985).
[2] R. Betti and J.P. Freidberg, Phys. Fluids B **3**, 1865 (1991).
[3] M.S. Chu *et al.*, Phys. Fluids B **4**, 3713 (1992).
[4] A.D. Turnbull *et al.*, Phys. Fluids B **5**, 2546 (1993).
[5] G.Y. Fu and J.W. Van Dam, Phys. Fluids B **1**, 2404 (1989).
[6] H.H. Duong *et al.*, Nucl. Fusion **33**, 749 (1993).
[7] K.L. Wong *et al.*, Phys. Rev. Lett. **66**, 1874 (1991).
[8] W.W. Heidbrink *et al.*, Nucl. Fusion **31**, 1635 (1991).
[9] S. Ali-Arshad and D.J. Campbell (to be published).
[10] W.W. Heidbrink *et al.*, Phys. Rev. Lett. **71**, 855 (1993).
[11] E. Fredrickson *et al.*, in Proceedings of XV International Conference on Plasma Physics and Controlled Fusion, IAEA, Seville, Spain, 1994 (unpublished).
[12] A. Fasoli *et al.*, in Ref. [11].
[13] G.A. Collins *et al.*, Phys. Fluids B **29**, 2260 (1986).
[14] G.A. Collins *et al.*, Plasma Controlled Fusion **29**, 324 (1987).
[15] P. Descamps *et al.*, Phys. Lett. A **143**, 313 (1990).
[16] G. Huysmans *et al.*, in *Proceedings of the XX European Conference on Controlled Fusion and Plasma Physics,* edited by J.A. Costa Cabral, M.E. Manso, F.M. Serra, and F.C. Schuller (EPS, Lisbon, 1993), Vol. I, p. 187.
[17] L. Villard *et al.*, in Ref. [16].
[18] J.-M. Moret, CRPP Laboratory Report No. LRP 498/94, 1994 (unpublished).
[19] L. Villard and G. Fu, Nucl. Fusion **32**, 1695 (1992).
[20] S. Poedts *et al.*, Plasma Phys. Controlled Fusion **34**, 1397 (1992).
[21] R. Betti and J.P. Freidberg, Phys. Fluids B **4**, 1465 (1992).
[22] N.N. Gorelenkov and S. Sharapov, Phys. Scr. **45**, 163 (1992).
[23] J. Candy and M.N. Rosenbluth, Plasma Phys. Controlled Fusion **35**, 957 (1993).
[24] R.R. Mett and S.M. Mahajan, Phys. Fluids B **4**, 2885 (1992).